Computational Investigation of Mass Transfer in Gas:Liquid Taylor flow

BTP Report Submitted in Partial Fulfilment

of the Requirement for the

Degree of Chemical Engineering

By

Anshul Patel

210107012

Under the guidance of

Prof. Raghvendra Gupta

DEPARTMENT OF CHEMICAL ENGINEERING

INDIAN INSTITUTE OF TECHNOLOGY, GUWAHATI

NORTH GUWAHATI, ASSAM-781039

DECLARATION

I certify that -

1. The research in this report is authentic and was carried out under my supervisor's leadership.
2. The report was not submitted for a degree or certificate to any other University.
3. I have agreed with the principles and criteria laid down in the Institute's Ethical Code of Conduct.
4. I have given credit to them if I have used resources from other sources (data, analytical analysis, figures, and script), citing them in the document text and the references for the information.

Date:

Signature

Name: ANSHUL PATEL

Acknowledgment

I am deeply thankful to my BTP supervisor Prof. Raghvendra Gupta, Department of Chemical Engineering, Indian Institute of Technology Guwahati for guiding me throughout the project and helped me to learn new concepts. I would also like to thank Mr. Mohammad Anzar Hussain, PhD student for his valuable assistance with my work.

Contents

Table of Figures

Chapter 1: Introduction

1.1. Background

Taylor flow, also referred to as slug flow or segmented flow, is a two-phase flow regime characterized by the alternating sequence of elongated gas bubbles and liquid slugs in confined channels. This flow pattern emerges as a dominant regime in microchannels due to the increased influence of interfacial forces over inertial forces at small scales. In Taylor flow, gas bubbles occupy nearly the entire cross-section of the channel, separated from the wall by a thin liquid film and from each other by liquid slugs.

The growing interest in Taylor flow stems from its practical significance in chemical engineering applications such as gas–liquid reactions, absorption, and catalysis. The segmented nature of the flow provides a high interfacial area for mass transfer, efficient mixing within the liquid slugs, and a reduction in axial dispersion, which is beneficial for process intensification and precise control over reaction environments.

1.2. Hydrodynamic Features and Flow Structure

The hydrodynamic structure of Taylor flow exhibits several distinctive features that significantly influence transport phenomena. These features include:

1. Bubble Morphology and Film Formation: Gas bubbles in Taylor flow typically adopt a bullet-like or capsule-like shape with hemispherical caps at both ends. The bubble is separated from the channel wall by a thin liquid film. This film thickness is a critical parameter affecting both hydrodynamics and mass transfer performance.
2. Recirculation Patterns in Liquid Slugs: One of the most significant features of Taylor flow is the development of toroidal vortices (recirculation zones) within the liquid slugs. When observed from a reference frame moving with the bubble, these recirculation patterns form due to the velocity differential between the central region of the slug and the near-wall region. The mixing intensity within these vortices is influenced by the bubble velocity, slug length, and channel geometry.
3. Bubble-to-Bubble Interactions: While individual unit cells (bubble-slug pairs) are often analysed in isolation, interactions between consecutive bubbles can influence the overall flow behaviour, particularly at shorter slug lengths or higher void fractions. These interactions manifest through perturbations in the velocity field and pressure distribution.

Channel geometry also plays a significant role. Smaller channels tend to produce shorter bubbles and higher velocities for a given flow rate, which can further enhance mass transfer by

increasing the number of unit cells (bubble-slug pairs) and the overall interfacial area. The distribution of film thickness—thinner at the channel centre and thicker at the corners in non-circular channels—can affect the local saturation and, consequently, the mass transfer dynamics.

1.3. Computational Fluid Dynamics (CFD) Approaches

Modern CFD techniques offer the most comprehensive approach to modelling mass transfer in Taylor flow, allowing for detailed resolution of the velocity and concentration fields throughout the system. Two principal CFD methodologies have emerged:

1. Stationary Domain Approach: This approach involves simulating a train of bubbles and slugs in the laboratory frame of reference using a time-dependent inlet boundary condition. While computationally intensive, this methodology allows for simultaneous modelling of hydrodynamic and mass transfer development along the channel length.
2. Moving Domain Approach: In this methodology, the simulation is performed in a reference frame moving with the bubble velocity, treating the flow as steady and focusing on a single unit cell with periodic boundary conditions. This approach is significantly more efficient computationally while still capturing the essential physics of the system.

1.4. Influence of Geometric Parameter

1. Channel Size and Shape: Smaller channels generally provide higher interfacial area-to-volume ratios, enhancing mass transfer. Channel cross-sectional geometry affects the film thickness distribution and recirculation patterns, with non-circular channels (square, rectangular, triangular) showing different mass transfer characteristics compared to circular channels.
2. Slug and Bubble Lengths: The liquid slug length significantly impacts mixing intensity and mass transfer efficiency. Shorter slugs typically lead to more intense recirculation but may increase pressure drop. The optimal slug length depends on the specific application requirements and fluid properties.
3. Film Thickness: Thinner films reduce the diffusion distance but may increase the risk of film rupture or bubble coalescence. The film thickness is primarily controlled through the Capillary number and can be adjusted by modifying the fluid properties or flow rates
4. Flow Rates and Velocity: Higher velocities generally enhance mass transfer by intensifying internal circulation in the slugs. However, this comes at the cost of reduced

residence time and increased pressure drop. The optimal velocity represents a balance between these competing factors

1.5. Applications and Future Perspectives

Taylor flow has found applications across numerous fields due to its favourable mass transfer characteristics. These applications include:

1. Gas-Liquid Reactions: Processes such as hydrogenation, oxidation, and carbonation benefit from the enhanced mass transfer and controlled residence time distribution offered by Taylor flow.
2. Absorption Processes: The high interfacial area and efficient mixing make Taylor flow attractive for gas absorption applications, including CO2 capture and gas purification.
3. Catalyst Coating in Capillaries: The regular flow pattern and thin liquid films in Taylor flow have been utilized for depositing catalyst coatings on microchannel walls with high uniformity.
4. Biological Applications: Taylor flow mimics some aspects of blood flow in capillaries and has been used to study oxygen transport and other biological mass transfer processes.
5. Heat Exchange with Phase Change: The principles governing mass transfer in Taylor flow also apply to heat transfer with phase change, relevant to applications like electronics cooling and refrigeration

1.6. Objective

1. To investigate the difference in mass transfer characteristics between the first and second bubbles in Taylor flow.
2. To determine how variations in flow conditions such as Reynolds number affect the mass transfer coefficient.
3. To determine the terminal velocity achieved by Taylor bubbles under varying flow conditions and to analyse the factors influencing this velocity.

Chapter 2: Computational Methodology

2.1. Volume of Fluid Method

To simulate the Taylor flow we utilized VoF (Volume of Fluid) in OpenFoam. The Volume of Fluid method is a numerical technique used to track and model the interface between two immiscible fluids (water and air) in Computational Fluid Dynamics simulations. The VoF method defines a volume fraction field, denoted by α, which represents the fraction of each fluid within a computational cell.

$\alpha = 0$, the cell contains air

$\alpha = 1$, the cell contains water

$0 < \alpha < 1$, the cell is at the interface between two fluids

Why Volume of Fluid Method?

The Volume of Fluid (VOF) method is ideal for bubble rising simulations as it accurately tracks the interface between gas and liquid phases, keeping a sharp boundary that is essential for capturing the bubble's shape and behaviour. Unlike other methods, VOF conserves mass effectively, ensuring that the bubble's volume remains constant during the simulation. It is computationally efficient, requiring only a single set of governing equations for the entire domain rather than separate equations for each phase, which reduces the computational effort. Moreover, VOF handles complex, deformable interfaces well, making it suitable for modelling the dynamic behaviour of bubbles as they rise and interact with the surrounding fluid. This combination of accuracy and efficiency makes VOF the preferred choice for such multiphase flow simulations.

2.2. Governing Equations

The VOF method is based on the Navier-Stokes equations, which describe the motion of fluid flow. The two main equations are:

1. **Continuity Equation**:

$$\frac{\partial \rho}{\partial t} + \nabla \cdot (\rho \vec{\boldsymbol{u}}) = 0 \qquad (2)$$

ρ: Fluid density (kg/m³).

$\boldsymbol{u}$: Velocity vector of the fluid (m/s).

t: Time (s).

2. **Momentum Equation**:

$$\frac{\partial(\rho\vec{u})}{\partial t} + \nabla \cdot (\rho\vec{u}\vec{u}) = -\nabla p + \nabla \cdot \mu(\nabla\vec{u}) + F_\sigma + \rho g \quad (3)$$

p: Pressure (Pa).

μ: Dynamic viscosity (Pa·s).

F_σ: Surface tension force.

ρg: Gravitational force.

The advection equation for the marker function or volume fraction of one of the phases α is given by,

$$\frac{\partial\alpha}{\partial t} + \nabla \cdot (\alpha\vec{u}) + \nabla \cdot (\alpha(1-\alpha)\vec{u_r}) = 0 \quad (4)$$

$\boldsymbol{u}$: Velocity field.

$(\boldsymbol{u_r})$: Relative velocity of the interface.

A: Volume fraction of the primary fluid.

The third term $\boldsymbol{\nabla \cdot (\alpha(1-\alpha)u_r)}$ is the compression term, used to reduce numerical diffusion at the interface. This term maintains a sharper interface by compressing the region where $0<\alpha<1$.

Now, to calculate the surface tension force working at the surface we have the following equation,

$$F_\sigma = \sigma\kappa n\delta_s \quad (5)$$

σ: Surface tension coefficient (N/m).

κ: Interface curvature.

N: Unit normal vector at the interface.

δ_s: Dirac delta function that is zero except at the interface.

To derive this equation:

We have the curvature as,

$$\kappa = -\nabla \cdot n \tag{6}$$

Where,

$$\mathrm{n} = \nabla\alpha/|\nabla\alpha| \tag{7}$$

The pressure drops across the interface is defined as,

$$\Delta p = \sigma\kappa \tag{8}$$

Hence, the force per unit volume will be,

$$F_\sigma = \sigma\kappa n\delta_s \tag{5}$$

The VoF method is generally very useful in simulations with two or more fluids. But it can suffer from numerical diffusion, where the interface between fluids becomes smeared or blurred, especially when the mesh is not fine enough.

2.3. Continuous Compressive Species Transfer (CCST) Method

To accurately model interfacial mass transfer in our Taylor flow simulations, the Continuous Compressive Species Transfer (CCST) method was implemented. This advanced technique enables precise tracking of species concentration across gas-liquid interfaces within the Volume of Fluid (VOF) framework.

The CCST method, an enhancement of the original Continuous Species Transfer (CST) approach developed by Haroun et al. and Marschall et al., addresses the fundamental challenge of representing concentration discontinuities at phase interfaces. While the original CST method provided a foundation for this modelling, it required extremely fine meshes to maintain accuracy at higher Peclet numbers.

In the implementation, the species transport equation was modified with additional terms to account for the concentration jump dictated by Henry's law:

$$\frac{\partial C_j}{\partial \mathrm{t}} + \nabla \cdot \left(C_j v + \left[\frac{(1-\mathrm{He})C_j}{\alpha + \mathrm{He}(1-\alpha)} \alpha(1-\alpha) v_r \right] \right) = \nabla \cdot \left(D_j \nabla C_j + \phi_j \right) \tag{9}$$

Where,

C_j: Concentration of chemical species j

v : Fluid velocity

α : Volume fraction ($0 \leq \alpha \leq 1$)

He: Henry's constant

v_r : Relative velocity (compression velocity)

D_j : Diffusivity

The key innovation in CCST is the inclusion of the compressive term (enclosed in square brackets above), which significantly improves numerical stability and accuracy at realistic mesh resolutions. This term effectively counteracts numerical diffusion at the interface, maintaining a sharp concentration profile.

Furthermore, instead of using a simple arithmetic average for diffusivity, an equilibrium-based mean diffusivity was employed:

$$D_j = \frac{\alpha D_{1j} + He(1-\alpha) D_{2j}}{\alpha + He(1-\alpha)} \quad (10)$$

This weighted average accounts for the differing diffusivities in both phases (D_{1j} and D_{2j}) properly balanced according to the volume fraction α and Henry's constant, providing a more physically accurate representation of the interfacial mass transfer process.

The CCST method was implemented using the interTransportFoam solver in OpenFOAM, which seamlessly integrates with the VOF method used for tracking the gas-liquid interface. This approach provided robust and accurate simulation of mass transfer across the interface in Taylor flow, capturing the concentration gradients essential for determining local and global mass transfer coefficients.

2.4. Geometry

Simulating an air bubble in a complete 3D cylindrical geometry requires large computation time, and refining a 3D mesh is challenging. To reduce computational load and streamline mesh refinement, the cylindrical geometry was converted into a 2D wedge. This transformation utilizes the axisymmetric of the cylinder, allowing for higher mesh resolution in critical regions without excessive computational costs. This approach ensures efficient modelling of bubble dynamics while maintaining the accuracy necessary for analysis.

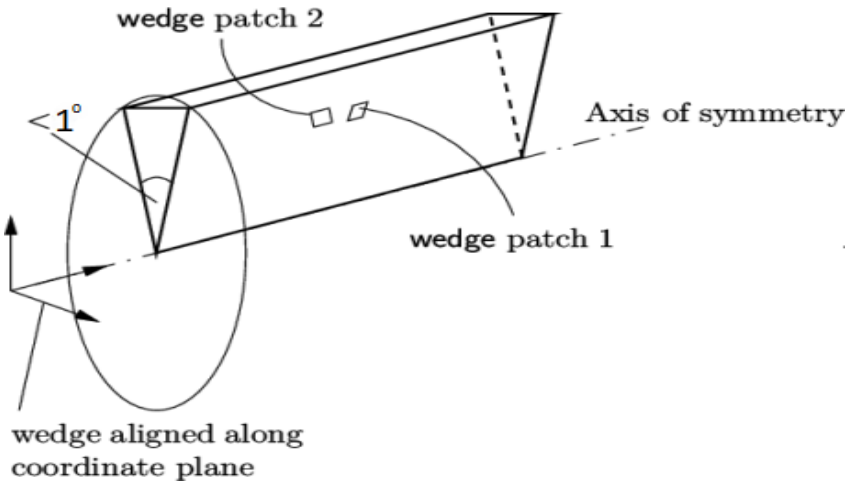

Figure 2-1:Image of geometry displaying axisymmetry of cylinder

The channel radius was taken to be 0.00025m and the gas inlet radius was taken 0.0002m. The length of the channel was taken 0.01m to properly capture the hydrodynamics and mass transfer.

2.5. Mesh

The computational mesh employed in this study was constructed with a uniform cell size of 2×10−62×10−6 meters. The mesh grid comprised 125 cells along the height and 5,000 cells along the length, resulting in overall mesh dimensions of 125 × 5,000. Consequently, the total number of cells in the computational domain amounted to 625,000. This fine mesh resolution was chosen to ensure accurate representation of the physical phenomena under investigation.

2.6. Initial and Boundary Conditions

For Pressure:

- *Initial Conditions:* The initial pressure throughout the computational domain is set to a uniform value of 0 Pa.
- *Boundary Conditions:* Atmospheric pressure was specified as a fixed uniform value of 0 Pa at the inlet boundaries. At the wall boundaries, a fixedFluxPressure condition was

applied, allowing the pressure to adjust according to the velocity field. At the outlet boundaries, a total pressure boundary condition with a value of 0 Pa was used to ensure appropriate outflow characteristics.

For Velocity:

- *Initial Conditions:* The initial velocity field was set to a uniform vector of (0, 0, 0) m/s across the entire domain.
- *Boundary Conditions*: A fixedValue boundary condition is applied at the inlet boundaries, specifying a uniform velocity of (0, 0.5, 0) m/s. At the outlet boundaries, a pressureInletOutletVelocity condition was used, permitting natural outflow without imposing a fixed velocity. The wall boundaries are defined with a no Slip condition, ensuring that the fluid velocity at the wall is zero.

For Alpha Water:

- *Initial Conditions:* The initial value of the water volume fraction was set to a uniform value of 1 throughout the computational domain.

- *Boundary Conditions*: At the gas inlet, a time-dependent coded boundary condition was applied, which dynamically alternates the water fraction between 0 and 1 based on the simulation time, allowing for the periodic entry of air and water phases. At the liquid inlet, a fixed value of 1 was specified to ensure that only water enters through this boundary. Both outlet boundaries were assigned an inletOutlet condition, enabling the phase fraction to exit the domain naturally while preventing any inflow from these boundaries. The wall boundary was set to a zeroGradient condition, allowing the phase fraction to be extrapolated from the interior without imposing a fixed value.

For Concentration:

- *Initial Conditions:* The initial value of the scalar field C was set to a uniform value of 0 throughout the computational domain, indicating that the gas is initially absent everywhere.

- *Boundary Conditions*: At the gas inlet, a time-dependent coded boundary condition was implemented similar to alpha water, which dynamically alternates the value of C between 1 and 0 based on the simulation time, allowing for periodic injection of the gas at this boundary. At the liquid inlet, a fixed value of 0 was specified, ensuring that no gas enters through this boundary. Both outlet boundaries were assigned an inletOutlet condition, enabling the gas to exit the domain naturally while preventing any inflow from these boundaries. The wall boundary was set to a globalConcentrationMixed condition with all reference values and sources set to zero, effectively imposing a no-flux condition for the gas at the wall.

2.7. Simulation Setup and Control Parameters

The simulation was conducted using the interTransportFoam solver, with the simulation time set so that at least one bubble passes through the simulation domain for different velocities. A small initial timestep of 0.0001 seconds was selected, and adaptive time stepping was enabled to maintain the Courant number below 0.2, ensuring numerical stability. Output data was written in adjustable intervals of 0.001 seconds, with results stored in ASCII format at a precision of 10 decimal places. The simulation settings were configured to be modifiable at runtime, allowing for flexible adjustments during execution.

2.8. Concentration and Velocity Calculation

To calculate the concentration and velocity of the bubble, the method used was based on integrating the velocity across all the cells occupied by the bubble. We focused on cells where the bubble was present, using the volume fraction, α, to identify the bubble region.

1. Identifying the Bubble Region: First we clipped out the cells in which the bubble under observation is present then using the isovolume function, we selected cells where the volume fraction α satisfied $0<\alpha<0.5$. This captured the area occupied by the bubble, ensuring we focused on the correct region for velocity calculations.
2. Averaging the Concentration or Velocity: The velocity in each of these selected cells was used to calculate the average velocity of the bubble. The equation for the average velocity, V_{avg}, is given by:

$$V_{avg} = (\sum_i n(u_i V_i))/(\sum_i n\ V_i) \quad (11)$$

Where:

u_i: Velocity in the i-th cell.

V_i: Volume of the i-th cell.

n: Total number of cells.

The same approach was applied for concentration calculations.

Chapter 3: Inlet Time and Mass Transfer Coefficient Calculation

3.1. Inlet Time Calculation

The volume of each gas bubble was set to $1.462\times10-10$ m³, while the corresponding liquid slug volume for each bubble was maintained at $2.466\times10-10$ m³. Based on these specified phase volumes, the inlet time for each velocity was subsequently calculated to ensure accurate and consistent introduction of both phases into the domain. This approach allowed for precise control over the bubble and slug formation dynamics within the simulation.

The following detailed calculations were performed to establish precise timing parameters for the bubble train flow at an inlet velocity of 0.5 m/s. These parameters are crucial for implementing the time-dependent boundary conditions in our simulation.

Volume of bubble (V_b): 1.462×10^{-10} m³

Volume of liquid slug (V_l): 2.466×10^{-10} m³

Superficial velocity (U): 0.5 m/s

Gas Phase Calculations:
To determine the duration of gas injection at the inlet, we first calculated the relevant parameters:
Gas inlet area (A_g): $\pi \times (0.0002)^2 = 1.257 \times 10^{-7}$ m²
Gas flux (Q_g): $U \times Ag = 0.5 \times 1.257 \times 10^{-7} = 6.283 \times 10^{-8}$ m³/s
Gas inlet time (t_g): $V_b / Q_g = 1.462 \times 10^{-10} / 6.283 \times 10^{-8} = 0.00232$ s

Liquid Phase Calculations:
During bubble formation, liquid flows in the annular region around the gas inlet.
Subsequently, a pure liquid slug follows each bubble:
Liquid flux with bubble: $0.5 \times \pi \times [(0.00025)^2 - (0.0002)^2] = 3.534 \times 10^{-8}$ m³/s
Volume of liquid with bubble: $3.534 \times 10^{-8} \times 0.00232 = 8.2 \times 10^{-11}$ m³
Volume of liquid slug in between: $2.466 \times 10^{-10} - 8.2 \times 10^{-11} = 1.646 \times 10^{-10}$ m³
Liquid flux (Q_l): $0.5 \times \pi \times (0.00025)^2 = 9.817 \times 10^{-8}$ m³/s
Liquid inlet time (t_l): $V_{l\_slug} / Q_l = 1.646 \times 10^{-10} / 9.817 \times 10^{-8} = 0.001676$ s

Total bubble cycle time:

The complete cycle time for a single bubble-slug unit was calculated as:

$t = t_g + t_l = 0.00232 + 0.001676 = 0.003996$ s

These timing parameters were directly implemented in the boundary conditions for the gas inlet to achieve the desired bubble train formation. The alternating pattern was accomplished by switching the alpha.water and C field values at the inlet according to these precisely calculated time intervals.

Table 1: Gas inlet and Liquid slug inlet time v/s Velocity

Velocity(m/s)	Gas inlet time(s)	Liquid slug inlet time(s)
0.3	0.00388	0.00279
0.4	0.00291	0.00209
0.5	0.00232	0.001676
0.7	0.00166	0.00119
0.85	0.00137	0.00098
1	0.00116	0.00084

3.2. Mass Transfer Coefficient Calculation

The overall gas-phase mass transfer coefficient was calculated using the logarithmic concentration ratio method, which is derived from the integrated form of the mass transfer rate equation. This approach provides a reliable determination of the coefficient from experimental or computational concentration data.

The mass transfer coefficient was calculated using the formula,

$$k_g a = \frac{1}{t} \ln \left(\frac{C_{g,0} - C^*_g}{C_{g,t} - C^*_g}\right) \quad (12)$$

Where,

k_g : Mass Transfer Coefficient

$C_{g,0}$: Concentration of species in gas at inlet

C^*_g : Saturation Concentration

$C_{g,t}$: Concentration of species in gas at time t

t : Time after entering domain

Chapter 4: Hydrodynamics of bubble

4.1. Terminal Velocity

Gas bubbles attain a terminal velocity exceeding the initial gas-phase velocity by approximately 10–15%, a phenomenon rooted in the unique hydrodynamics of confined two-phase flow. This velocity enhancement arises from complex interactions between interfacial forces, liquid recirculation, and pressure gradients.

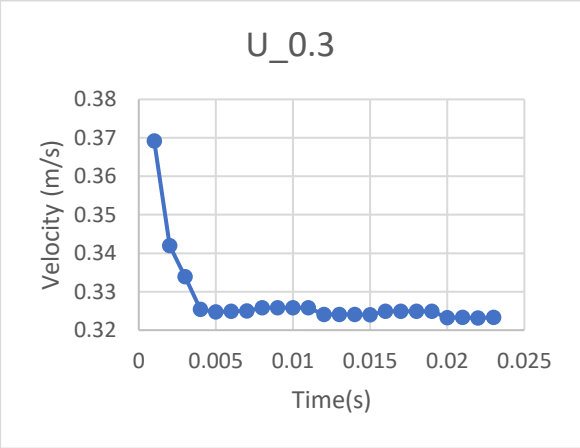

(a)

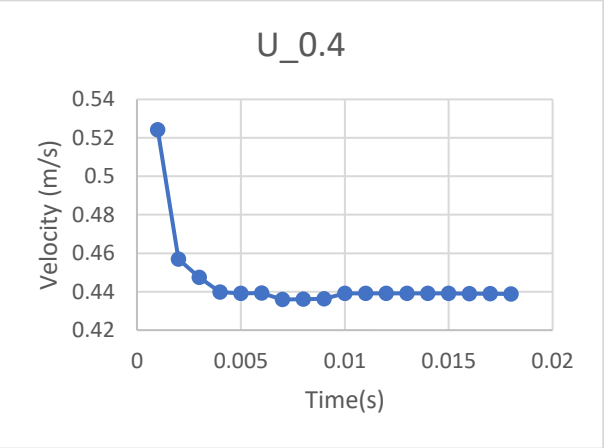

(b)

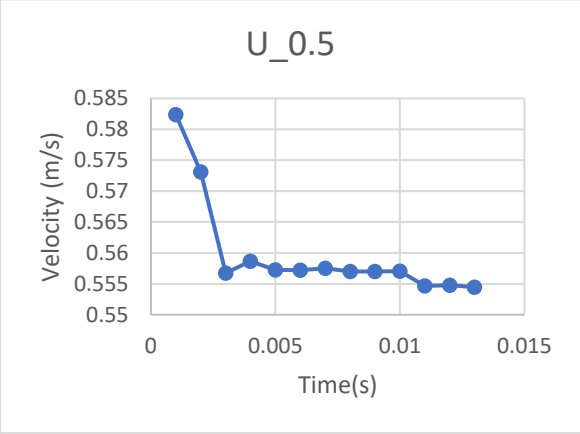

(c)

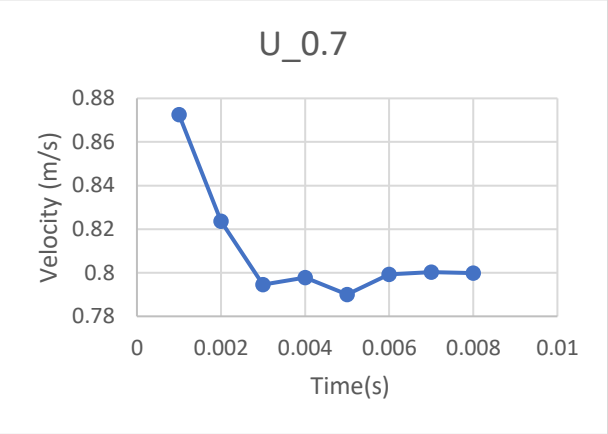

(d)

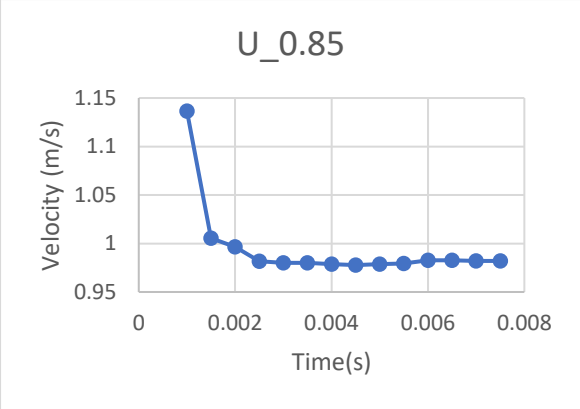

(e)

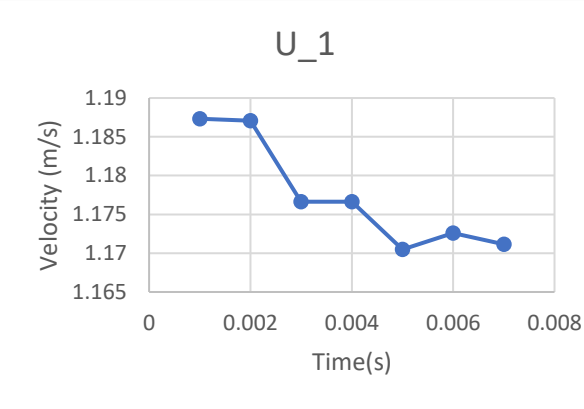

(f)

Figure 4-1: Velocity v/s Time graphs for different velocities (a) 0.3 m/s (b) 0.4 m/s (c) 0.5 m/s (d) 0.7 m/s (e) 0.85 m/s (f) 1 m/s

Table 2: Initial Velocity V/s Terminal Velocity Table

Initial Velocity	Terminal Velocity
0.3 m/s	0.325 m/s
0.4 m/s	0.44 m/s
0.5 m/s	0.555 m/s
0.7 m/s	0.8 m/s
0.85 m/s	0.98 m/s
1 m/s	1.17 m/s

4.2. Flow Field

The streamlines in the simulation clearly show the presence of a vortex within the liquid slug between two consecutive bubbles. This recirculation zone is a hallmark of Taylor flow and matches theoretical predictions and previous experimental observations. The formation of these vortices is due to the velocity difference between the faster-moving bubble and the surrounding liquid, which induces a shear-driven flow pattern. As a result, liquid circulates within the slug, moving upward along the channel centreline and downward near the channel wall, creating a closed-loop or vortex structure.

Observing this vortex in the streamline plots confirms that the simulation is capturing the expected hydrodynamic behaviour of Taylor flow. The presence of these recirculation zones is significant because they enhance mixing within the liquid slug and promote efficient mass transfer at the gas-liquid interface, both of which are important for applications involving heat and mass transfer in microchannels.

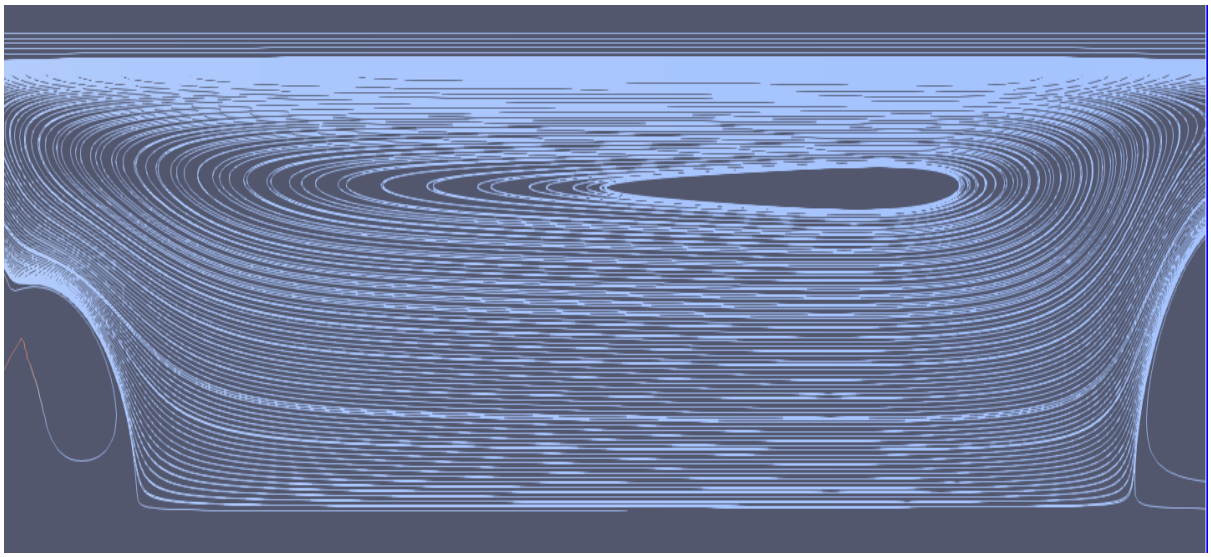

Figure 4-2: Image showing streamline between the bubbles

4.3. Film Thickness

The film thickness observed in the simulation was 9.24 µm, which is in very good agreement with theoretical and experimental values reported in the literature for Taylor flow. Classical correlations such as those by Fairbrother and Stubbs, Taylor, and Bretherton predict film thicknesses in the range of 10 to 11 µm for comparable Capillary numbers. More recent studies, including those by Aussillous and Quere, Klaseboer et al., Gupta et al., and Butler et al., also report values between 10 and 12 µm. In this work, the simulated film thickness of 9.24 µm is close to these theoretical predictions and previous experimental results, confirming the accuracy of the hydrodynamic modelling and interface capturing in my simulation. This close match demonstrates that the Volume of Fluid (VOF) method used here is capable of reliably capturing the thin liquid film dynamics that are characteristic of Taylor flow in microchannels.

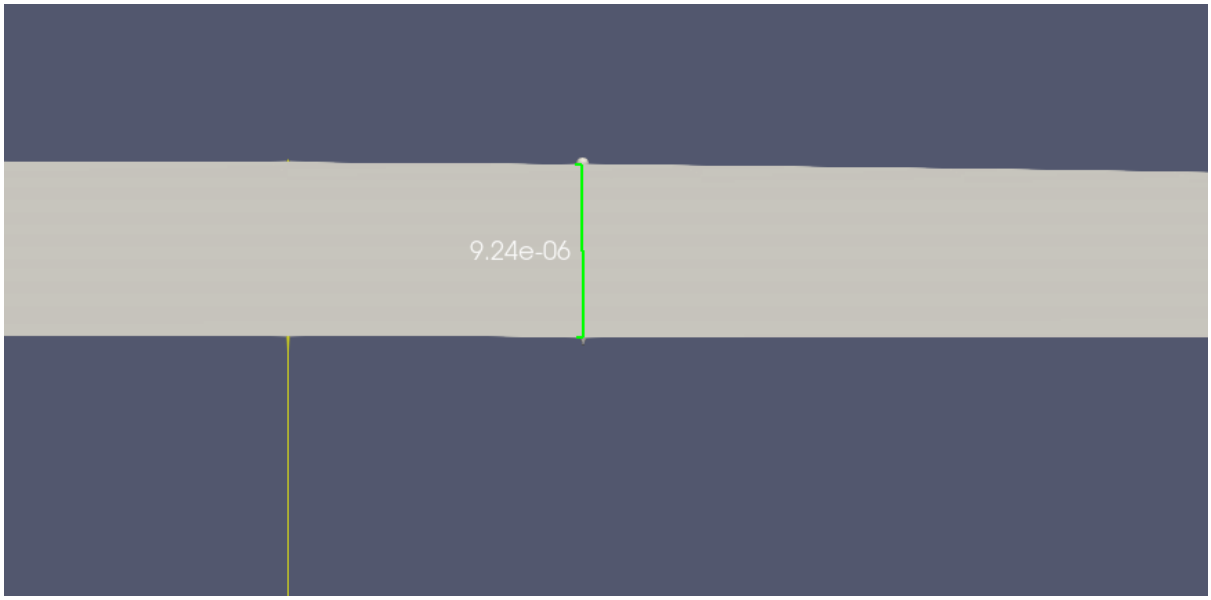

Figure 4-3: Image showing the film thickness of bubble

Chapter 5: Mass Transfer

5.1. Mass Transfer Coefficient

Difference in MTC in bubble 1&2:

The experimental results reveal a significant disparity in mass transfer coefficients between bubble 1 and bubble 2 in the Taylor flow regime. Bubble 1 exhibits a substantially higher mass transfer coefficient compared to bubble 2. This phenomenon can be attributed to the concentration gradient dynamics that govern mass transfer processes in gas-liquid systems.

For bubble 1, the initial concentration gradient is maximized as it encounters virgin liquid containing no dissolved species. This creates an optimal driving force for mass transfer according to Fick's law, where the flux is directly proportional to the concentration gradient. The absence of any pre-dissolved species in the liquid phase surrounding bubble 1 maintains this steep gradient throughout the initial mass transfer process, resulting in enhanced transfer rates.

In contrast, bubble 2 travels through liquid that has already been partially saturated by the preceding bubble. This partial saturation reduces the concentration differential between the gas in bubble 2 and the surrounding liquid phase, thereby diminishing the driving force for mass transfer.

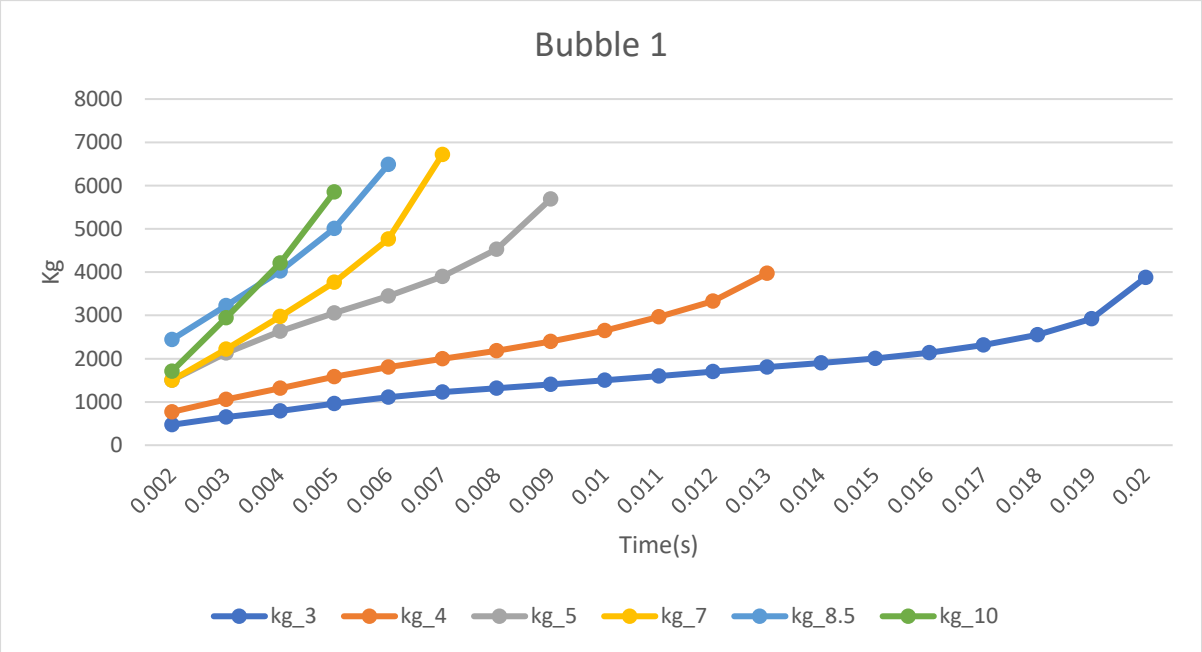

Figure 5-1: Mass Transfer Coefficient v/s Time for bubble 1

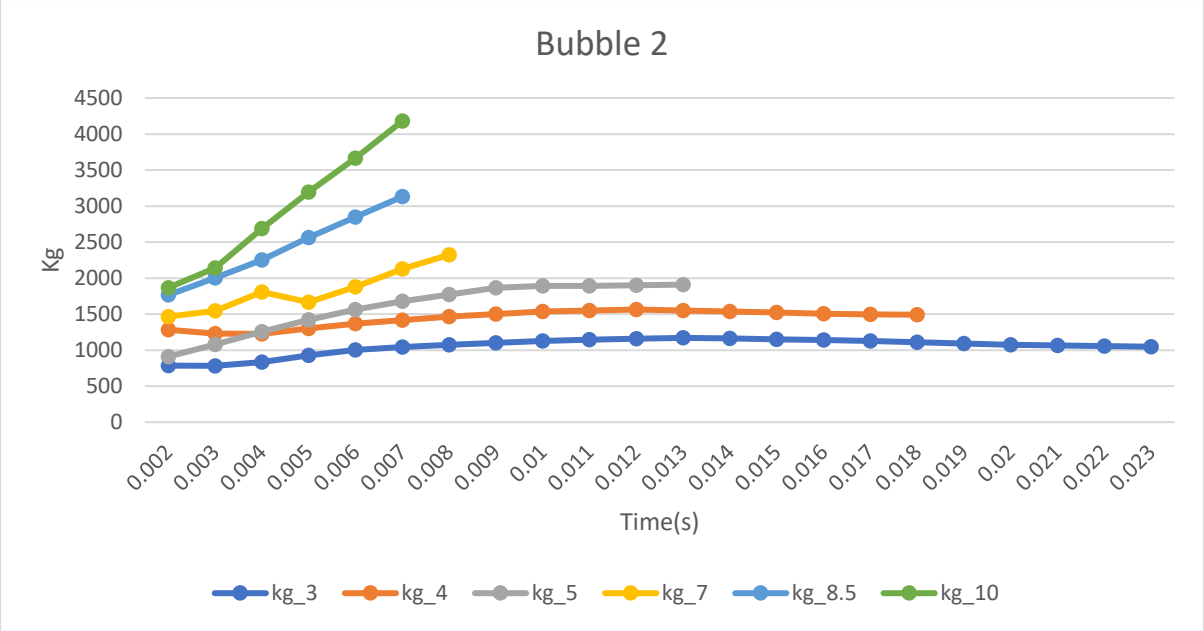

Figure 5-2: Mass Transfer Coefficient v/s Time for bubble 2

Effect of Reynolds Number:

It was also observed that the mass transfer coefficient increases as the Reynolds number increases. This trend can be explained by the fact that a higher Reynolds number corresponds to a greater flow velocity and, consequently, more intense recirculation within the liquid slugs. As the Reynolds number rises, the enhanced internal circulation promotes more effective mixing and frequent renewal of the liquid at the gas–liquid interface. This reduces the thickness of the concentration boundary layer, leading to a steeper concentration gradient at the interface and thus a higher rate of mass transfer. Additionally, higher Reynolds numbers can decrease the residence time of the liquid in the slug, but the overall effect is an improvement in the mass transfer coefficient due to the more vigorous convective transport. This relationship between Reynolds number and mass transfer is well established in the literature and is consistent with the hydrodynamic behaviour observed in Taylor flow systems.

5.2. Concentration

From the graph below, it is evident that the reduction in concentration for bubble 1 is significantly greater than that for bubble 2. This can be attributed to the initially high concentration gradient experienced by bubble 1, as it interacts with unsaturated liquid, resulting in a more pronounced mass transfer. In contrast, bubble 2 encounters liquid that has already been partially saturated by bubble 1, leading to a reduced concentration gradient and, consequently, a lower rate of mass transfer.

Additionally, the results indicate that cases with higher Reynolds numbers exhibit a more substantial reduction in concentration. This is due to the enhanced convective mixing and increased recirculation within the liquid slugs at higher Reynolds numbers, which promote more efficient mass transfer from the bubble to the surrounding liquid.

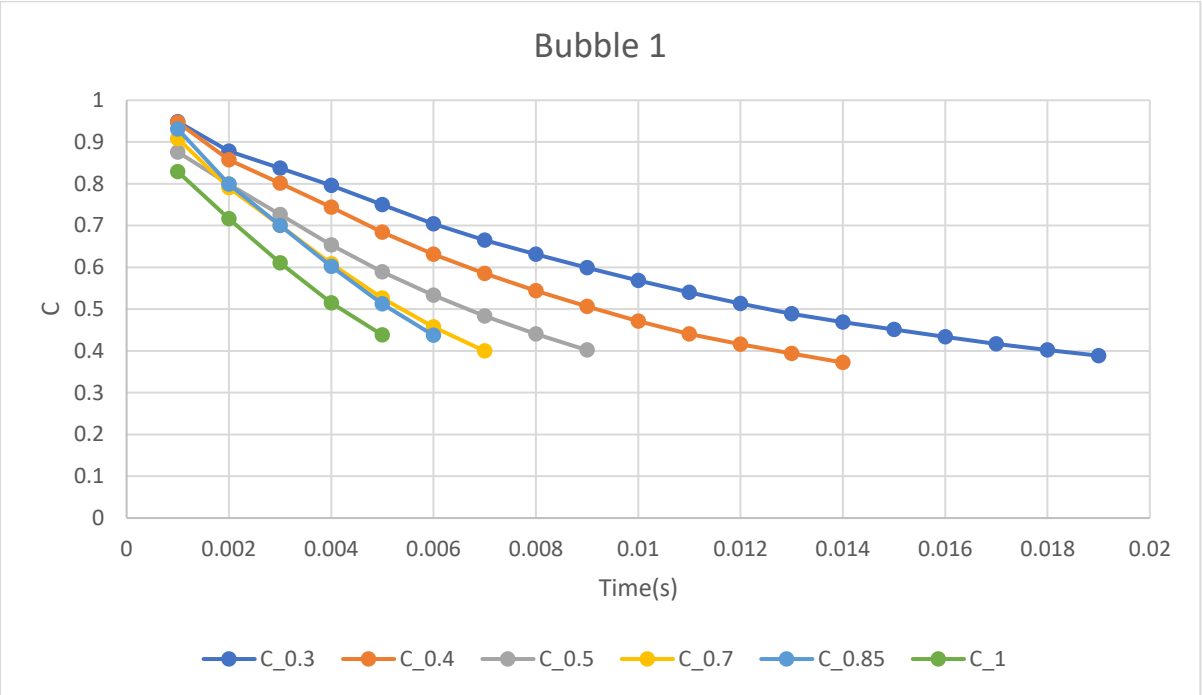

Figure 5-3: Concentration v/s Time for bubble 1

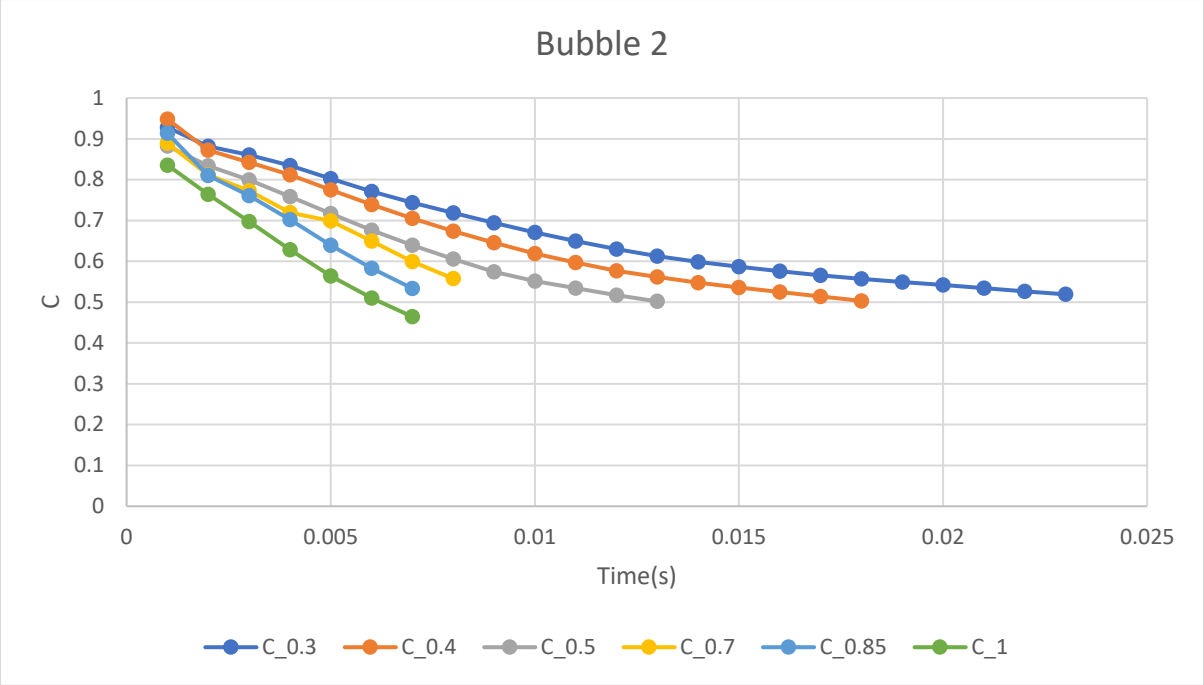

Figure 5-4: Concentration v/s Time for bubble 2

Chapter 6: Future Work

- Study the impact of curved or serpentine microchannel geometries on both hydrodynamics and mass transfer, as these configurations are common in practical microreactors and could significantly affect bubble dynamics and mass transfer rates
- Investigate the coupling between heat and mass transfer in Taylor flow, particularly how temperature gradients affect mass transfer coefficients and interfacial dynamics.
- Study the evolution of mass transfer over extended time periods to capture saturation effects and concentration profile development throughout longer channel sections

Appendix

The Taylor flow simulations in this study were performed using OpenFOAM with an axisymmetric geometry. The computational setup includes all essential OpenFOAM directories: the 0 folder containing initial and boundary conditions, the system folder with solver settings and numerical schemes, and the constant folder specifying physical properties and mesh details. These files collectively define the simulation environment and ensure reproducibility of the results. For reference and transparency, all relevant OpenFOAM case files used in this work are organized and made available at the following link:

Files Link

References

[1] Mohammad Anzar Hussain, Raghvendra Gupta (2024). Development and Validation of a Computational Methodology to Model Mass Transfer in Gas–Liquid Taylor Flow in a Circular Microchannel. Industrial & Engineering Chemistry Research.

[2] Clive William Hirt, Billy Dean Nichols (1981). Volume of Fluid (VOF) Method for the Dynamics of Free Boundaries. Journal of Computational Physics.

[3] Raghvendra Gupta, David Francis Fletcher, Brian Stuart Haynes (2010). Taylor Flow in Microchannels: A Review of Experimental and Computational Work. Journal of Computational Multiphase Flows.

[4] Azadeh Nazanin Asadolahi, Raghvendra Gupta, David Francis Fletcher, Brian Stuart Haynes (2011). CFD Approaches for the Simulation of Hydrodynamics and Heat Transfer in Taylor Flow.

[5] Nan Shao, Asterios Gavriilidis, Panagiota Angeli (2010). Mass Transfer during Taylor Flow in Microchannels with and without Chemical Reaction. Chemical Engineering Journal, Chemical Engineering Science.

[6] Thazhe Chirayil Thulasidas, Martin Allen Abraham, Ricardo Luis Cerro (1997). Flow Patterns in Liquid Slugs during Bubble-Train Flow inside Capillaries. Chemical Engineering Science.

.